IET Microwaves, Antennas & Propagation

Research Article

Analysis of multi-port amplifier calibration for optimal magnitude and phase error detection

ISSN 1751-8725
Received on 8th September 2014
Revised on 8th August 2015
Accepted on 27th August 2015
doi: 10.1049/iet-map.2015.0237
www.ietdl.org

Han Lim Lee[1], Moon-Que Lee[2] ✉, Jong-Won Yu[3]

[1]*School of Electrical and Electronics Engineering, Chung-Ang University, 84 Heukseok-ro, Dongjak-gu, Seoul 156-756, South Korea*
[2]*School of Electrical Engineering and Computer Science, UOS, Siripdae-Gil 13, Dongdaemun-Gu, Seoul 130-743, South Korea*
[3]*Department of Electrical Engineering, KAIST, 291 Daehak-ro, Yuseong-Gu, Daejeon 305-701, South Korea*
✉ *E-mail: mqlee@uos.ac.kr*

Abstract: This study presents theoretical analysis and verification on optimal hardware platform for calibration of signal manipulation in multi-port amplifier (MPA). Since MPA output power and isolation characteristics are strongly dependent on magnitude and relative phase balances in each array path of MPA, proper calibration technique is necessary for ideal MPA operation. Although variety of calibration methods can be considered, they can be classified into two methods from the calibration signal detection based on hardware platform point of view. That is, calibration signals for each array path in MPA can be sampled and detected before output hybrid matrix (OHM) or after OHM according to hardware setup. Since optimal signal detection for each array path is the key to ideal MPA calibration and maximised performance, this study theoretically analyses two different calibration hardware platforms detecting calibration signals. Then, the mathematically derived optimal calibration hardware setup for detecting magnitude and phase error is finally verified and concluded by simple simulation and measurement at 900 MHz Industrial, Scientific and Medical-band (902–928 MHz).

1 Introduction

Modern and future satellite communication systems require high degree of performance flexibility within a long lifetime of satellites such as diversity in antenna coverage and efficiency in power allocation [1, 2]. To increase the system flexibility, there have been many approaches including phase array antenna-based architecture which is not considered as economically suitable for Ku- or Ka-band system [3]. Among various techniques to effectively control multiple communication traffics over the lifetime of satellite, multi-port amplifier (MPA) can be an attractive solution and has been studied as an effective approach in multi-beam system [4]. Comparing with the conventional power amplification structures, MPA architecture has advantages in power flexibility including the increase in maximum output power and power allocation range, and lower DC power consumption by the use of shared power amplifiers (PA) with lower saturation power [1]. However, since the electrical array paths of MPA are connected by input hybrid matrix (IHM) and output hybrid matrix (OHM), the performance of MPA critically depends on the proper recombination of amplified signals from each array path in MPA. As seen from Fig. 1, each input signal with different channel frequency is amplified by multiple PAs and then recombined to the corresponding outputs, resulting in multi-beam generations for different coverage regions based on multiple inputs and multiple outputs operation. In order for MPA to operate ideally, magnitude and phase relations in each signal path should be balanced. Otherwise, signals cannot be recombined properly into the corresponding outputs and additionally, leakages to adjacent output ports are generated. Consequently, degradations in port-to-port isolation and unwanted output power loss occur.

To ensure the good isolation and output power characteristics of MPA, a calibration circuitry is necessary and is generally included in MPA for optimising the system performance by compensating unwanted deviations in electrical performance of PAs. From the calibration hardware point of view, MPA structure can be classified as shown in Fig. 2 such as MPA without calibration block, MPA with manual calibration and MPA with automatic calibration. For calibration circuitry, voltage-controlled phase shifters and voltage-controlled attenuators are generally needed to adjust the phase and magnitude balances in each path as shown in Figs. 2*b* and *c*. Moreover, additional calibration control block to adjust the phase shifters and attenuators is required for automatic MPA calibration as shown in Fig. 2*c*.

Although there have been several calibration schemes [5–9] proposed previously, they all have the shortcomings in finding specific signal path among arrays including unwanted electrical performance variation, and distinguishing the phase and magnitude errors in each signal path. In more detail, since most calibration schemes sample the signals required for calibration process from OHM outputs where all signals are already recombined as shown in Fig. 3*a*, errors cannot be distinguished whether they come from magnitude mismatch or phase mismatch or combination of both magnitude and phase mismatches. Moreover, the array path including the corresponding magnitude or phase errors cannot be directly found.

To solve the problems by the calibration architectures based on Fig. 3*a*, a new calibration method that can distinguish the source of error and manage phase and magnitude errors separately has been conceptually proposed in [10] as shown in Fig. 3*b*. According to Fig. 3*b*, the calibration circuitry detects signals in each path of array before the signal combination happens by OHM and thus the sampled signals still have each array path's magnitude and phase information. Since the magnitude and phase deviations in each path can be directly compared, direct correction for the corresponding errors to degrade overall system performance seems to be made. However, the previously proposed research lacks theoretical analysis that can support the advantage of detecting signals before OHM mathematically and more importantly the calibration scheme does not include the magnitude and phase of OHM in the calibration process. That is, the effect of uncalibrated OHM on MPA isolation and output power characteristics is not analysed. Thus, in this paper, two different MPA calibration hardware configurations as described in Fig. 3 are theoretically analysed first to investigate the best MPA calibration hardware platform. Then, the effect of OHM not taken into account for the previous report [10] as in Fig. 3*b* is further investigated with 4×4 Butler matrix waveguide measurement to

conclude whether this method can be the optimal MPA calibration or not from hardware platform point of view.

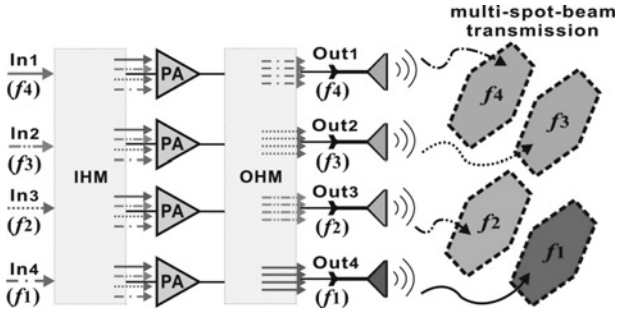

Fig. 1 *General description of MPA operation (4 × 4 case)*

2 Theoretical analysis

2.1 Ideal MPA operation

For ideal MPA operation, the magnitude of each array path should be identical to each other and the relative phase differences among array paths should be 0°, −90°, −90° and −180° for 4 × 4 MPA structure. Referring to Fig. 2*a*, electrical performance deviations of each PA are defined by G_1, G_2, G_3, G_4, ϕ_1, ϕ_2, ϕ_3 and ϕ_4 where G and ϕ denote gain and relative phase change by PA, respectively, while electrical performance variations by IHM and OHM implemented as passive networks are assumed to be negligible. Then, if the electrical characteristics of each PA are the same ($G_1 = G_2 = G_3 = G_4 = G$ and $\phi_1 = \phi_2 = \phi_3 = \phi_4 = \phi$), the ideal MPA operation can be expressed as follows

$$\mathrm{Out}_1 = D \cdot G \cdot \mathrm{e}^{-\mathrm{j}\pi}, \quad \mathrm{Out}_2 = \mathrm{Out}_3 = \mathrm{Out}_4 = 0 \tag{1}$$

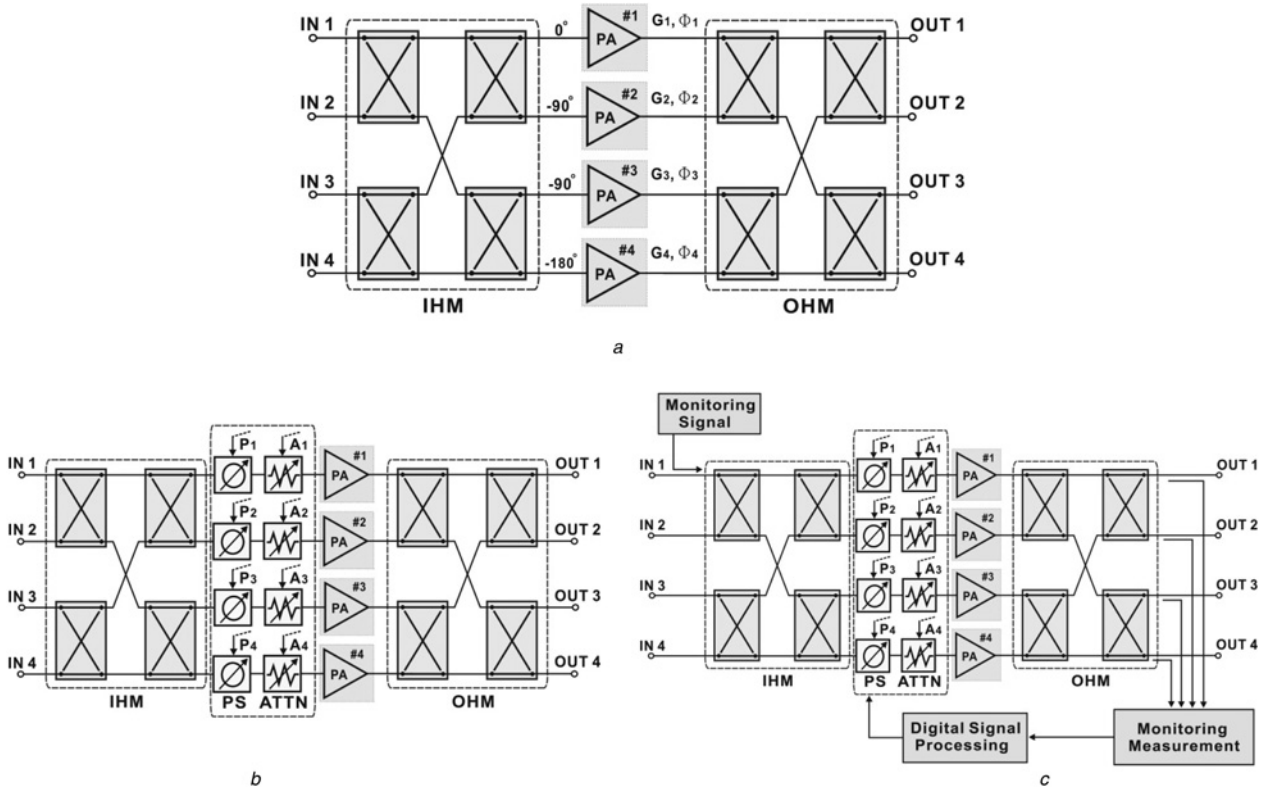

Fig. 2 *MPA classifications by calibration hardware point of view (4 × 4 case)*

a No calibration
b Manual calibration
c Automatic calibration

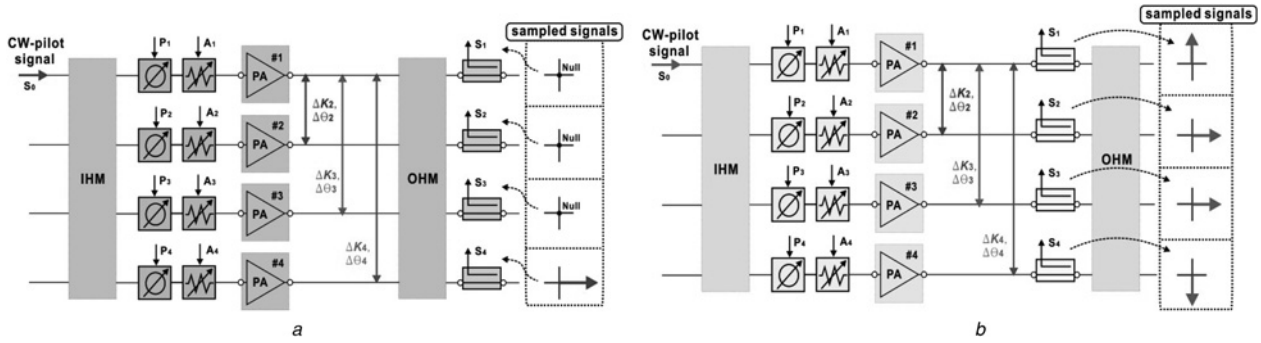

Fig. 3 *Two different calibration signal detection schemes according to the location of signal couplers (4 × 4 case)*

a Coupler placement after OHM
b Coupler placement before OHM

$$\mathrm{Out}_2 = C \cdot G \cdot \mathrm{e}^{-\mathrm{j}\pi}, \quad \mathrm{Out}_1 = \mathrm{Out}_3 = \mathrm{Out}_4 = 0 \tag{2}$$

$$\mathrm{Out}_3 = B \cdot G \cdot \mathrm{e}^{-\mathrm{j}\pi}, \quad \mathrm{Out}_1 = \mathrm{Out}_2 = \mathrm{Out}_4 = 0 \tag{3}$$

$$\mathrm{Out}_4 = A \cdot G \cdot \mathrm{e}^{-\mathrm{j}\pi}, \quad \mathrm{Out}_1 = \mathrm{Out}_2 = \mathrm{Out}_3 = 0 \tag{4}$$

For example, according to (4), the incident signal to input A is amplified by the gain of PA and then outputted to Out_4 while the rest of output ports are null in ideal MPA. Similarly, each amplified signal (B, C or D at different frequencies) is only generated to a single corresponding output port and the rest of output ports produce no powers. Since the port-to-port isolation is determined by the output power difference between the port in use and the rest of ports not in use, the MPA isolation for ideal operation should be maximum. In addition, since all signals are in balance and ideally combined through OHM, output combining loss should be minimum.

2.2 MPA operation by magnitude and phase imbalance

Referring to Fig. 2*a*, if the electrical characteristics of each PA are not identical ($G_1 \neq G_2 \neq G_3 \neq G_4$ and $\phi_1 \neq \phi_2 \neq \phi_3 \neq \phi_4$), then the 4×4 MPA no longer operates ideally as expressed by (5) and outputs with respect to inputs are determined as follows (see (5))

Since G and Φ of each PA are not balanced, the terms in (5) cannot be summed or cancelled appropriately, resulting in non-ideal recombination to desired output ports and leakage generations to unwanted output ports. For example, according to (5) for $N = 1$, the terms related to A, B and C inputs need to be cancelled out while the terms related to D should be summed up only if $G_1 = G_2 = G_3 = G_4$ and $\phi_1 = \phi_2 = \phi_3 = \phi_4$. However, if electrical deviations occur such as $G_1 \neq G_2 \neq G_3 \neq G_4$ and $\phi_1 \neq \phi_2 \neq \phi_3 \neq \phi_4$, Out_1 is no longer the pure summation of the terms related to D and the leakages from other inputs are produced. Moreover, D is not only recombined to Out_1 but leaks to other output ports. That is, the desired output power decreases and the isolation characteristics are also degraded due to the leakage generations.

2.3 Effect of gain and phase deviations by PAs

To find the changes in output power and isolation characteristics of MPA, general 4×4 MPA case is investigated with the assumption that each gain and phase deviations occur uniformly with respect to each signal path as shown below

$$|G_1 - G_2| = |G_2 - G_3| = |G_3 - G_4| = \Delta G \tag{6}$$

$$|\phi_1 - \phi_2| = |\phi_2 - \phi_3| = |\phi_3 - \phi_4| = \Delta\phi, \tag{7}$$

where G_1, G_2, G_3, G_4, ϕ_1, ϕ_2, ϕ_3 and ϕ_4 are indicated as in Fig. 2*a*. Although uniform deviations are assumed, approximate combining loss and isolation characteristics can still be predicted as long as the deviation ranges are wide enough. Using advanced design system (ADS), gain and phase variations are adjusted by built-in phase shifter and attenuator models and applied to the ideal 4×4 MPA in order to draw contour plots of their effect. Fig. 4 shows the effect of combining loss variation by the gain and phase deviations. As both gain and phase deviations get greater, combining loss gets greater as well. It is noted that the combining loss characteristic is more susceptible to gain deviations and the gain deviation should be <1.2 dB in order to satisfy the combining loss <1 dB. Moreover, Fig. 5 shows the changes in isolation characteristic by gain and phase deviations. As both gain and phase deviations get greater, the isolation gets degraded. However, the isolation characteristic is severely affected by both gain and phase deviations comparing with the combining loss characteristic in Fig. 4. According to both Figs. 4 and 5, gain deviation <1.2 dB and phase deviation <13° are required to satisfy the combining loss of < 1 dB and the isolation better than 25 dB.

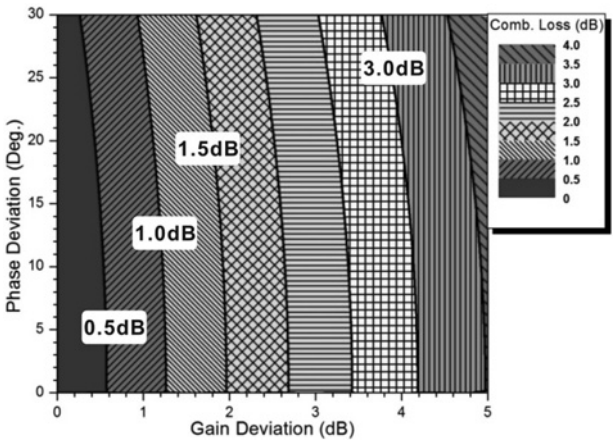

Fig. 4 *Combining loss variation by gain and phase deviations for general 4 × 4 MPA configuration*

2.4 MPA calibration by signal detection after OHM

As seen previously, gain and phase deviations should be minimised and corrected to optimal path balance for ideal MPA operation. Thus, magnitude and phase calibrations for each array path are necessary, and the array paths of MPA should be precisely analysed so as to calibrate MPA ideally. The first calibration configuration is to detect array path signals after OHM as shown in Fig. 3*a* where directional couplers are placed after OHM. Referring to Fig. 3*a*, the gain and phase deviations of each path corresponding to PA1, 2, 3 and 4 are G_1, G_2, G_3, G_4 and ϕ_1, ϕ_2, ϕ_3, ϕ_4, respectively. Then, the relative gain and phase differences among each path can be represented as follows

$$K_2 = \frac{G_2}{G_1}, \quad K_3 = \frac{G_3}{G_1}, \quad K_4 = \frac{G_4}{G_1} \tag{8}$$

$$\theta_2 = \phi_2 - \phi_1, \quad \theta_3 = \phi_3 - \phi_1, \quad \theta_4 = \phi_4 - \phi_1. \tag{9}$$

$$\begin{aligned}\mathrm{Out}_N = \frac{1}{4} \cdot \big[& A \cdot \left(G_1 \cdot \mathrm{e}^{-\mathrm{j}(\phi_1 + p \cdot \pi/2)} + G_2 \cdot \mathrm{e}^{-\mathrm{j}\{\phi_2 + (q+1) \cdot \pi/2\}} + G_3 \cdot \mathrm{e}^{-\mathrm{j}\{\phi_3 + (r+1) \cdot \pi/2\}} + G_4 \cdot \mathrm{e}^{-\mathrm{j}\{\phi_4 + (s+2) \cdot \pi/2\}}\right) \\ & + B \cdot \left(G_1 \cdot \mathrm{e}^{-\mathrm{j}\{\phi_1 + (p+1) \cdot \pi/2\}} + G_2 \cdot \mathrm{e}^{-\mathrm{j}\{\phi_2 + (q+2) \cdot \pi/2\}} + G_3 \cdot \mathrm{e}^{-\mathrm{j}(\phi_3 + r \cdot \pi/2)} + G_4 \cdot \mathrm{e}^{-\mathrm{j}\{\phi_4 + (s+1) \cdot \pi/2\}}\right) \\ & + C \cdot \left(G_1 \cdot \mathrm{e}^{-\mathrm{j}\phi_1 + (p+1) \cdot \pi/2\}} + G_2 \cdot \mathrm{e}^{-\mathrm{j}\phi_2 + q \cdot \pi/2)} + G_3 \cdot \mathrm{e}^{-\mathrm{j}\phi_3 + (r+2) \cdot \pi/2\}} + G_4 \cdot \mathrm{e}^{-\mathrm{j}\{\phi_4 + (s+1) \cdot \pi/2\}}\right) \\ & + D \cdot \left(G_1 \cdot \mathrm{e}^{-\mathrm{j}\{\phi_1 + (p+2) \cdot \pi/2\}} + G_2 \cdot \mathrm{e}^{-\mathrm{j}\phi_2 + (q+1) \cdot \pi/2\}} + G_3 \cdot \mathrm{e}^{-\mathrm{j}\phi_3 + (r+1) \cdot \pi/2\}} + G_4 \cdot \mathrm{e}^{-\mathrm{j}_4 + s \cdot \pi/2)}\right)\big]; \\ & p = 0, q = 1, \quad r = 1, s = 2 \text{ for } N = 1 \\ & p = 1, q = 2, \quad r = 0, s = 1 \text{ for } N = 2 \\ & p = 1, q = 0, \quad r = 2, s = 1 \text{ for } N = 3 \\ & p = 2, q = 1, \quad r = 1, s = 0 \text{ for } N = 4.\end{aligned} \tag{5}$$

IET Microw. Antennas Propag., 2016, Vol. 10, Iss. 1, pp. 102–110

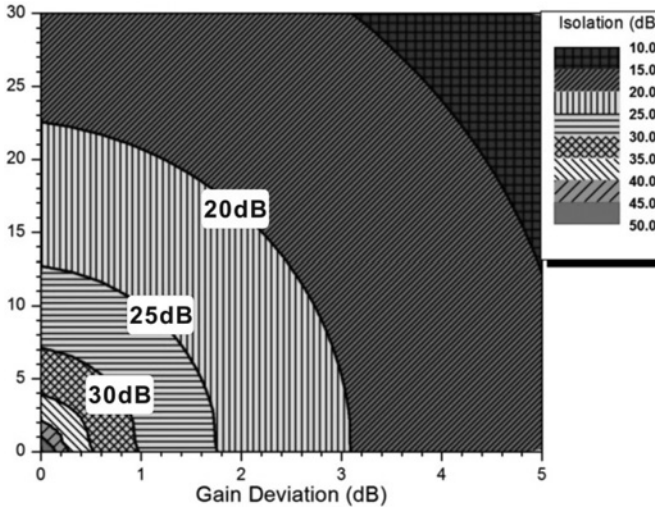

Fig. 5 *Port-to-port isolation variation by gain and phase deviations for general 4 × 4 MPA configuration*

By solving the matrices in Fig. 3*a*, the sampled signals S_1, S_2, S_3 and S_4 with respect to the continuous wave (CW)-pilot signal, S_0, can be found as follows

$$\begin{aligned} S_N &= \frac{x}{4}\cdot S_0\left(G_1 e^{-j\phi_1} + a\cdot G_2 e^{-j\phi_2} + b\cdot G_3 e^{-j\phi_3} + c\cdot G_4 e^{-j\phi_4}\right) \\ &= \frac{x}{4}\cdot S_0\cdot G_1\cdot e^{-j\phi_1}\left(1 + a\cdot K_2\cdot e^{-j\theta_2} + b\cdot K_3\cdot e^{-j\theta_3} + c\cdot K_4\cdot e^{-j\theta_4}\right); \\ & x=1, \quad a=-1, \quad b=-1, \quad c=1 \quad \text{for } N=1 \\ & x=-j, \quad a=-1, \quad b=1, \quad c=-1 \quad \text{for } N=2 \\ & x=-j, \quad a=1, \quad b=-1, \quad c=-1 \quad \text{for } N=3 \\ & x=-1, \quad a=1, \quad b=1, \quad c=1 \quad \text{for } N=4. \end{aligned} \tag{10}$$

Since the detected signals are sampled at the output ports where signal recombination is already taken place, only the power of detected signals can be compared with each other so as to find the point where the power at the wanted output port is the maximum and the powers at the unwanted output ports (the ports supposed to be null ideally) are the minimum. Thus, the relative power comparisons among the detected signals at the output ports can be rearranged and expressed as shown by

$$\begin{aligned} S_{|\mathrm{MAG}|N} &= 16\cdot\frac{|S_N|^2}{|G_1\cdot S_0|^2} \\ &= \left(1 + a\cdot K_2\cos\theta_2 + b\cdot K_3\cos\theta_3 + c\cdot K_4\cos\theta_4\right)^2 \\ &\quad + \left(a\cdot K_2\sin\theta_2 + b\cdot K_3\sin\theta_3 + c\cdot K_4\sin\theta_4\right)^2; \\ & a=-1, \quad b=-1, \quad c=1 \quad \text{for } N=1 \\ & a=-1, \quad b=1, \quad c=-1 \quad \text{for } N=2 \\ & a=1, \quad b=-1, \quad c=-1 \quad \text{for } N=3 \\ & a=1, \quad b=1, \quad c=1 \quad \text{for } N=4. \end{aligned} \tag{11}$$

Since the calibration needs to adjust optimal phase and attenuation level for each phase shifter and attenuator by observing the sampled output powers, (11) should be solved for finding the maximum at the desired output port while finding the minima at the rest of output ports. However, since only four equations are available and six variables (K_2, K_3, K_4, θ_2, θ_3 and θ_4) need to be found, the method by detecting signals after OHM can hardly find the optimal calibration points. To find the possible maximum and minimum output powers with respect to the six variables, partial derivatives of (11) with respect to all K_2, K_3, K_4, θ_2, θ_3 and θ_4 must be taken as follows

$$\begin{aligned} \frac{\partial S_{|\mathrm{MAG}|N}}{\partial K_2} = \frac{\partial S_{|\mathrm{MAG}|N}}{\partial K_3} = \frac{\partial S_{|\mathrm{MAG}|N}}{\partial K_4} = \frac{\partial S_{|\mathrm{MAG}|N}}{\partial \theta_2} = \frac{\partial S_{|\mathrm{MAG}|N}}{\partial \theta_3} \\ = \frac{\partial S_{|\mathrm{MAG}|N}}{\partial \theta_4} = 0, \quad N = 1, 2, 3, 4. \end{aligned} \tag{12}$$

However, each equation corresponding to $N=1,2,3$ and 4 might have different values of K_2, K_3, K_4, θ_2, θ_3 and θ_4 for making the corresponding output powers minimum or maximum because each variable is inter-related throughout all equations. For instance, the values found in the case of $N=1$ might not be able to maintain optimal calibration for other output ports ($N=2$, 3 or 4). If the case of $N=1$ from (12) is taken as an example to solve for finding K_2 and θ_2, the following can be observed

$$\begin{aligned} \frac{\partial S_{\mathrm{MAG1}}}{\partial K_2} = 0 \Rightarrow K_2 \\ = \cos\theta_2 - K_3\cos(\theta_2 - \theta_3) + K_4\cos(\theta_2 - \theta_4) \end{aligned} \tag{13}$$

$$\frac{\partial S_{\mathrm{MAG1}}}{\partial \theta_2} = 0 \Rightarrow \theta_2 = \tan^{-1}\left(\frac{K_4\sin\theta_4 - K_3\sin\theta_3}{1 - K_3\cos\theta_3 + K_4\cos\theta_4}\right). \tag{14}$$

Looking into (13) and (14), solutions for each variable are co-related with other variables and thus exact values cannot be directly obtained. Moreover, calculations similar to (13) and (14) must be iterated for all conditions in (12). Therefore, the calibration method by detecting signals after OHM undergoes severe drawbacks such as complicated calculations or algorithms, long calibration time due to large amount of calculations and difficulty in finding optimal calibration points due to the lack of equations for solving necessary variables. That is, the signal detection after OHM cannot be an optimal calibration method. 2.5 MPA calibration by signal detection before OHMComparing with the calibration configuration shown in Fig. 3*a*, the directional couplers for sampling calibration signals are placed before OHM as shown in Fig. 3*b*. Again, the gain and phase deviations of each path corresponding to PA1, 2, 3 and 4 are denoted as G_1, G_2, G_3, G_4 and ϕ_1, ϕ_2, ϕ_3, ϕ_4, respectively. Equations (8) and (9) are applied to indicate the relative gain and phase deviations from each path. Then, the sampled signals S_1, S_2, S_3 and S_4 with respect to the CW-pilot signal, S_0, can be found as follows

$$\begin{aligned} S_N &= \frac{x}{2}\cdot S_0\cdot G_N\cdot e^{-j\phi_N}; x = 1 \text{ for } N = 1, x = -j \text{ for } N \\ &= 2, 3 \text{ and } x = -1 \text{ for } N = 4. \end{aligned} \tag{15}$$

Unlike the sampled signals after OHM, the amplified signals detected before OHM are not yet recombined through OHM and thus the magnitude and phase of each array paths are found independently to other paths. That is, relative gain and phase deviations among the array paths can be directly compared as shown in Fig. 6, resulting in accurate correction of magnitude and phase errors to the corresponding array path. That is, the ideal MPA condition referring to (8) and (9), $K_2 = K_3 = K_4 = 1$ and $\theta_2 = \theta_3 = \pi/2$, $\theta_4 = \pi$ can be quickly and precisely achieved by adjusting attenuators and phase shifters in the corresponding array paths.

3 Measurement results

To compare the efficiency of two different calibration approaches, 4 × 4 MPA was implemented at 900 MHz Industrial, Scientific and Medical (ISM) band for the ease of verification. The 4 × 4 MPA was configured with two 4 × 4 Butler matrices as IHM and OHM, phase shifters and attenuators, drive amplifiers and 10 dB

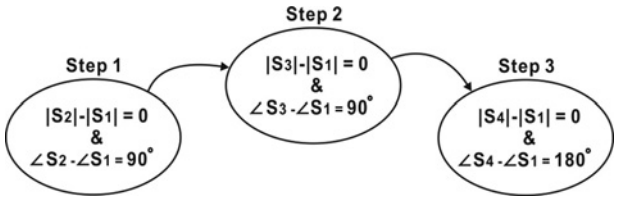

Fig. 6 *Simplified calibration steps made possible by signal detection before OHM*

directional couplers as shown in Fig. 3 where PA was replaced by drive amplifiers for measurement purpose.

3.1 4 × 4 Hybrid coupler, phase shifter and attenuator design and measurement

The 4 × 4 Butler matrices, designed as IHM and OHM, were shown in Fig. 2, where commercially available LTCC 3 dB couplers were used. Fig. 7 shows the measured *S*-parameters. Port 1 was used as an input port while ports 5, 6, 7 and 8 were used as output ports. The measured transmission loss variations of the 4 × 4 Butler matrix outputs were <1.1 dB as shown in Fig. 7*a* and the measured phase variations from the ideal phase differences among the output ports (0°, −90°, −90° and −180°) were <2° from 800 MHz to 1 GHz as shown in Fig. 7*b*. Moreover, the isolations were better than 28 dB and return losses were always better than 33 dB at 900 MHz ISM band (902–928 MHz).

For quick estimation, the combining loss contour plot and isolation contour plot as shown in Figs. 4 and 5 can be referred to predict the approximate performance of the calibration technique with the real OHM. On the basis of the plots, even though OHM is not included in the calibration, the isolation characteristic better than 30 dB and the combining loss characteristic better than 1.0 dB can be approximated.

To adjust the gain and phase deviations in 4 × 4 MPA, reflection-type voltage-controlled phase shifter and attenuator were designed and measured at the centre frequency of 900 MHz ISM band as shown in Figs. 8 and 9. The phase shifter used varactor diode where the variation of capacitance was controlled by applied voltage, resulting in phase shift. Moreover, the attenuator used PIN diode where resistance of PIN diode was controlled by applied voltage, resulting in attenuation. As shown in Fig. 8*b*, the maximum phase shift could be achieved up to 90° by varying voltages from 0 to 4 V while the insertion loss variation was <0.2 dB during the phase shift. As shown in Fig. 9*b*, the maximum attenuation of 10 dB could be achieved by varying voltages from 0 to 0.7 V while the phase variation during the attenuation was <4°.

3.2 Hybrid simulation by using simulation models and measurement data

Although the calibration method by detecting signals before OHM could directly adjust corresponding magnitude and phases in each array path, the effect of OHM was not taken into account when the sampled signals were processed for path calibration. That is, in order to verify the signal detection before OHM as an optimal calibration method, the output performance affected by the exclusion of OHM for calibration should also be investigated. In order to verify the prediction and practical performance of the calibration method detecting signals before OHM, hybrid simulation test was set as shown in Fig. 10. In the hybrid simulation test, ADS was again used where the measured OHM were imported and simulated with ideal built-in amplifier, phase shifter and attenuator ADS models so as to see the pure effect of uncalibrated OHM on the MPA calibration result. For the ease of test verification, the values of phase shifter and attenuator ADS models were set to make each array path in balance as if calibration was conducted excluding only OHM. That is, the electrical characteristics of each array path were adjusted to have equal magnitude and ideal phase differences (0°, −90°, −90° and −180°) at each frequency by setting of phase shifter and attenuator models in the ADS simulation manually in order to only reflect the effect of OHM after calibration. This hybrid simulation test was valid since we assumed that the ideal calibration was performed up to the OHM and we were only interested in how the uncalibrated OHM affects the electrical performances of MPA such as combining loss and isolation among output ports.

Fig. 11 shows that the combining loss over the operation band (902–928 MHz) was <0.6 dB and the output isolations were better than 30 dB over the operation band. That is, although the calibration method detecting signals before OHM did not include OHM in the calibration process, the effects of OHM in terms of combining loss and isolation characteristics were not significant.

3.3 Comparison of the calibration methods by measurement

To compare the efficiency of two calibration approaches where calibration signals were sampled before and after OHM, respectively, the measurements were conducted with the designed IHM, OHM, phase shifter, attenuator and commercially available drive amplifier and 10 dB directional coupler as shown in Fig. 12.

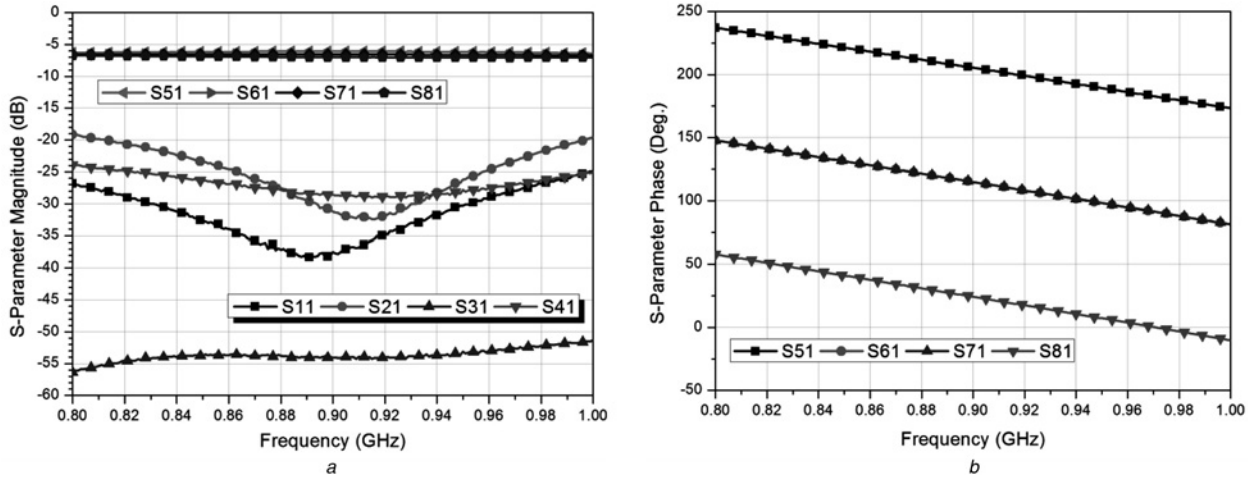

Fig. 7 *Measured S-parameters of the 4 × 4 Butler matrix*

a Transmission, return and isolation characteristics
b Output phase characteristics

IET Microw. Antennas Propag., 2016, Vol. 10, Iss. 1, pp. 102–110

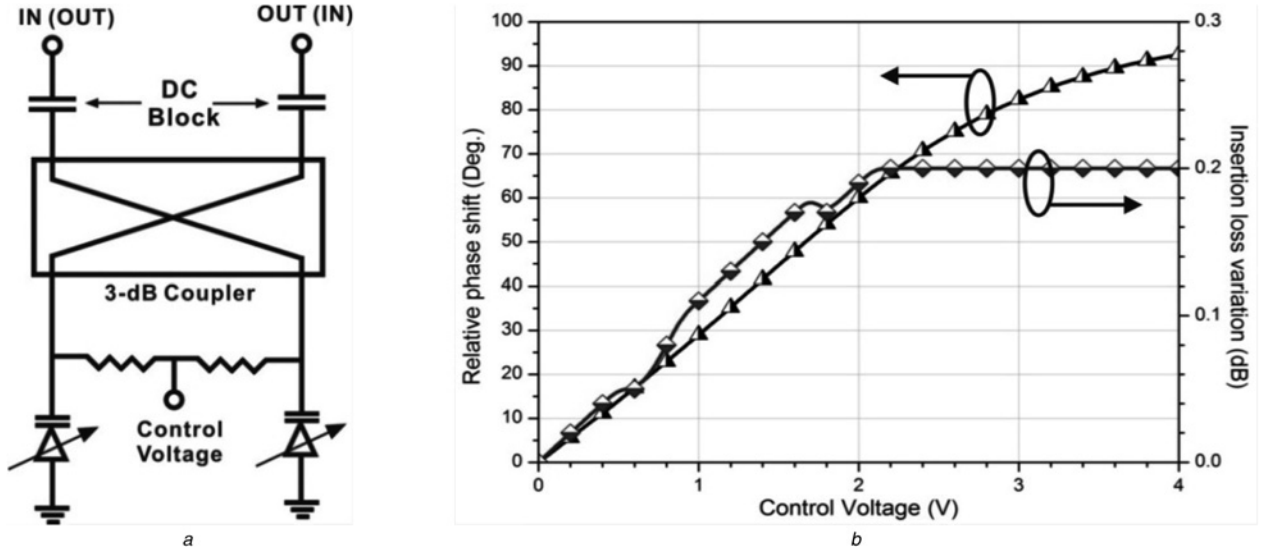

Fig. 8 *Reflection-type voltage-controlled phase shifter*

a Schematic of the designed phase shifter
b Phase shift and insertion loss variation characteristics according to control voltage

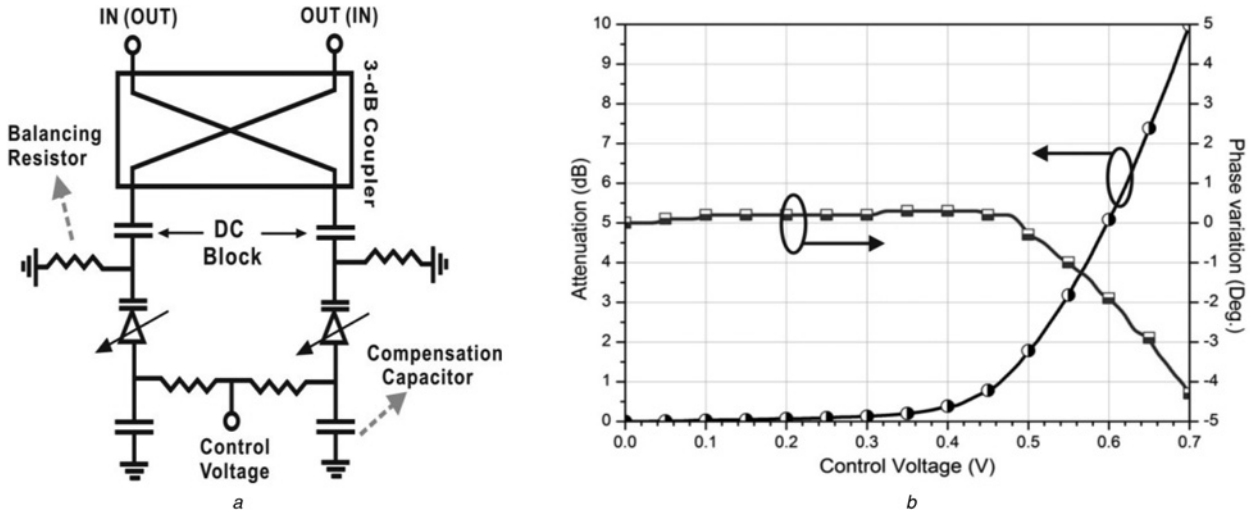

Fig. 9 *Reflection-type voltage-controlled attenuator*

a Schematic of the designed attenuator
b Attenuation and phase variation characteristics according to control voltage

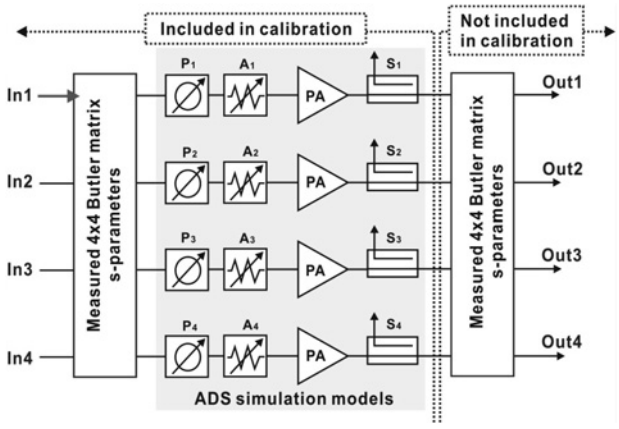

Fig. 10 *Hybrid simulation test setup where measurement data and simulation models are used together*

The drive amplifier had a gain of 19 dB, an input return loss of 20 dB and an output return loss of 21 dB at 915 MHz. For the ease of measurement, vector network analyser was used to monitor the sampled calibration signals.

Fig. 13 shows the measurement of the uncalibrated 4 × 4 MPA performance where In_4, Out_1, Out_2, Out_3 and Out_4 could be referred to Fig. 10. Here, the uncalibrated MPA showed output power of 15.4 dBm and isolation of about 24 dB at 915 MHz.

To calibrate the magnitude and phase deviation as shown in Fig. 13, the first approach that detected sampled signals after OHM was conducted and the measured results were shown in Fig. 14. Here, 10 dB directional coupler was placed after OHM and thus only relative magnitudes of the sampled signals could be monitored. We randomly adjusted phase shifters and attenuators until maximum isolation characteristic seemed to be reached. The measured isolation was about 27.2 dB where 3.2 dB was improved from the uncalibrated isolation. Moreover, the measured output power was about 15.1 dBm at 915 MHz.

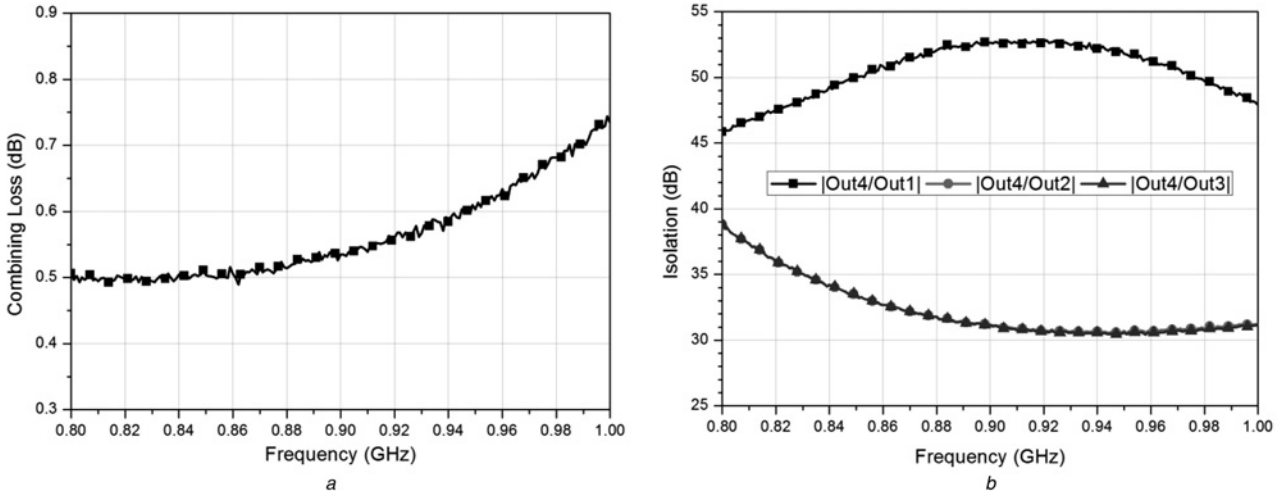

Fig. 11 *Hybrid simulation test results of the 4 × 4 MPA using the calibration method detecting signals before OHM*

a Combining loss
b Isolation characteristics

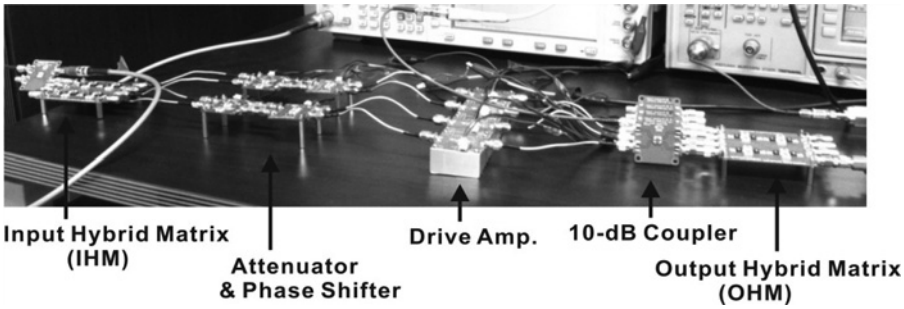

Fig. 12 *Measurement setup for 4 × 4 MPA at 900 MHz ISM band*

Finally, the second approach that detected sampled signals before OHM was conducted. Since both magnitudes and phases of the sampled signals could be monitored, the calibration steps described in Fig. 6 could be followed. Fig. 15 showed the measured isolation characteristics as well as the sampled signals before and after the calibration. Here, paths 1, 2, 3 and 4 corresponded to the paths to Out_1, Out_2, Out_3 and Out_4, respectively. Figs. 15*a* and *c* showed the sampled magnitude and phase before the calibration where the magnitude deviation was about 1.0 dB and the relative phase deviation from the ideal phase difference was about 4° in the operation band. Figs. 15*b* and *d* showed the sampled magnitude and phase after the calibration where the magnitude and phase balances were within 0.05 dB and 0.5° in the operation band. Having the 4 × 4 MPA calibrated, the measured isolation was about 30.2 dB where 6.2 dB was improved from the uncalibrated isolation and the measured output power was 14.9 dBm.

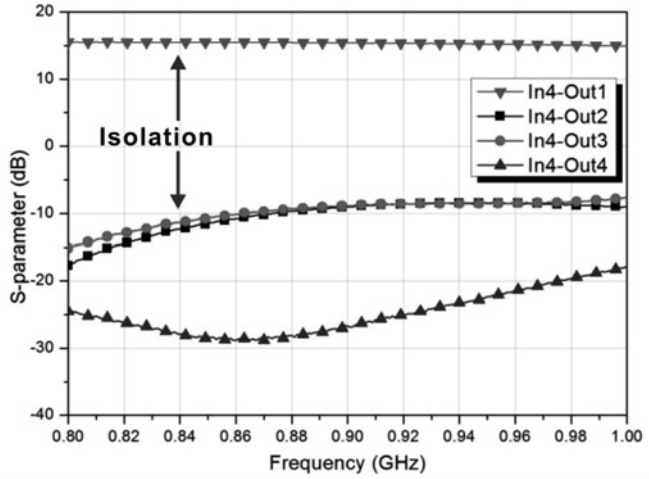

Fig. 13 *Measured 4 × 4 MPA isolation characteristics before calibration*

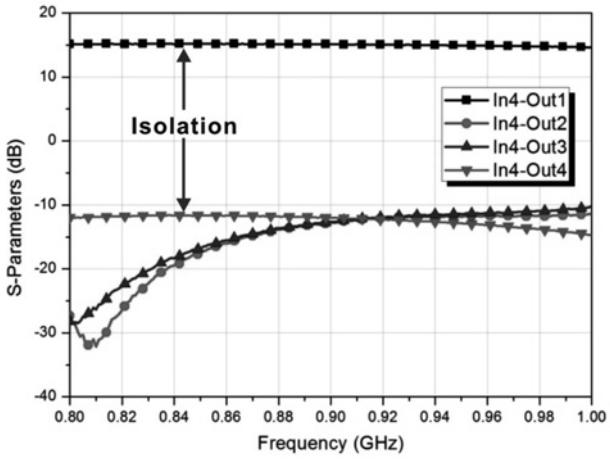

Fig. 14 *Measured 4 × 4 MPA performance after using the first calibration method where signals were sampled after OHM*

IET Microw. Antennas Propag., 2016, Vol. 10, Iss. 1, pp. 102–110

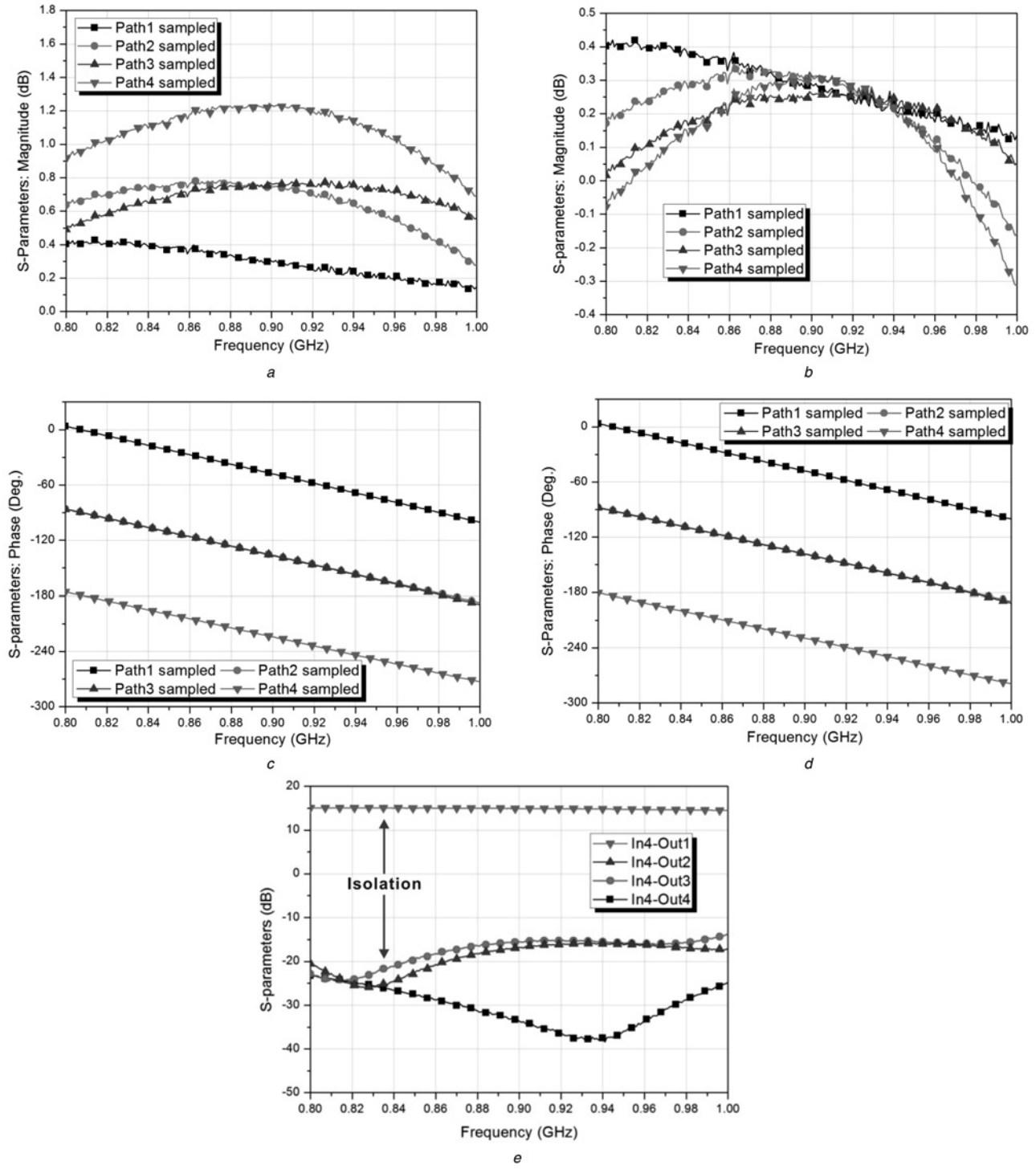

Fig. 15 *Measured 4 × 4 MPA performance after using the second calibration method where signals were sampled before OHM*

a Sampled magnitude measurement before calibration
b Sampled magnitude measurement after calibration
c Sampled phase measurement before calibration
d Sampled phase measurement after calibration
e Measured isolation characteristic after calibration

By comparing the measured results, the calibration approach detecting sampled signals before OHM showed better isolation performance as well as the ease of calibration process.

4 Conclusion

To maximise the effective use of MPA, a calibration circuitry that can accurately correct magnitude and phase deviations in the array path of MPA should be included. Although there have been several calibration methods proposed previously, calibration signal sampling hardware platforms can be divided into two ways: signal detection after OHM and before OHM. Therefore, this paper first theoretically analysed two different calibration platforms based on the calibration signal detections to find out the optimal calibration configuration for MPA. The calibration configuration detecting signals after OHM could not avoid complicated and long calculations because of the insufficient information on magnitude

and phase deviations. On the other hand, the calibration configuration detecting signals before OHM could simplify the required calculations but OHM was not taken into account for calibration. Thus, the pure effect of OHM on MPA performance was also analysed and estimated by the integration of calibrated blocks and uncalibrated 4×4 Butler matrix through a hybrid simulation test. Furthermore, the two approaches were tested at 900 MHz ISM band by designing and using reflection-type phase shifter and attenuator and commercially available 10 dB directional coupler and drive amplifier. The measured results showed that the calibration hardware platform detecting signals before OHM as the optimal calibration technique.

5 References

1 Mallet, A., Anakabe, A., Sombrin, J., *et al.*: 'Multiport-amplifier based architecture versus classical architecture for space telecommunication payloads', *IEEE Trans. Microw. Theory Tech.*, 2006, **54**, (12), pp. 4353–4361

2 Park, U., Kim, H.W., Oh, D.S., *et al.*: 'A dynamic bandwidth allocation scheme for a multi-spot-beam satellite system', *ETRI J.*, 2012, **34**, (4), pp. 613–616

3 Seong, N., Pyo, C., Chae, J., *et al.*: 'Ka-band satellite active phased array multi-beam antenna'. IEEE 59th Vehicular Technology Conf., May 2004, vol. 5, pp. 2807–2810

4 Egami, S., Kawai, M.: 'An adaptive multiple beam system concept', *IEEE J. Sel. Area Commun.*, 1987, **5**, (4), pp. 630–636

5 Huang, X., Caron, M.: 'Self-calibrating multi-port circuit and method'. US Patent Application US20080143562, 2008

6 Zhu, Z., Huang, X., Caron, M.: 'Ka-band multi-port power amplifier calibration experiment and results'. Second Int. Conf. on Advances in Satellite Space Communications, June 2010, pp. 11–14

7 Kaho, T., Yamaguchi, Y., Nakagawa, T., *et al.*: 'Adaptive linearization technique for multi-port amplifier'. Proc. Asia Pacific Microwave Conf., December 2006, pp. 895–898

8 Zhu, Z., Huang, X.: 'Multi-port power amplifier calibration estimation technique based on ICA algorithm'. Third Int. Conf. on Advances in Satellite Space Communication, April 2011, pp. 20–23

9 Christian, T., Soulie, J.-M.: 'Multi-port amplification device that self-compensates in the presence of traffic'. US Patent US20120280748, 2012

10 Moon, S.-M., Shin, D.-H., Lee, H.-Y., *et al.*: 'Adaptive calibration method in mulitport amplifier for K-band payload applications', *ETRI J.*, 2013, **35**, (4), pp. 718–721